A NONLINEAR FINITE ELEMENT FRAMEWORK FOR VISCOELASTIC BEAMS BASED ON THE HIGH–ORDER REDDY BEAM THEORY

G. S. PAYETTE AND J. N. REDDY

Abstract. A weak form Galerkin finite element model for the nonlinear quasi-static and fully transient analysis of initially straight viscoelastic beams is developed using the kinematic assumptions of the third-order Reddy beam theory. The formulation assumes linear viscoelastic material properties and is applicable to problems involving small strains and moderate rotations. The viscoelastic constitutive equations are efficiently discretized using the trapezoidal rule in conjunction with a two-point recurrence formula. Locking is avoided through the use of standard low order reduced integration elements as well through the employment of a family of elements constructed using high polynomial-order Lagrange and Hermite interpolation functions.

1. Introduction

Materials exhibiting characteristics of both elastic solids as well as viscous fluids are commonly known as viscoelastic materials. Prominent examples include metals at elevated temperatures, polymers, rubbers and concrete. The theoretical foundations of viscoelasticity are well established. We refer to the standard texts of Flügge [14], Christensen [9], Findley [13] and Reddy [36] for an overview on the theory of viscoelastic material behavior, as well as the classical analytical solution techniques that may be used to solve simple viscoelastic boundary value problems. Viscoelastic materials are often highly desirable for use in structural components, due to their natural ability to dampen out structural vibrations. The capability to satisfactory predict the mechanical response of viscoelastic structures therefore becomes of great importance in engineering design scenarios.

A variety of beam theory based finite element models have been presented in the literature for the analysis of viscoelastic structures. The majority of these formulations employ some form of either the Euler-Bernoulli or Timoshenko beam theories and are mostly restricted to small strain analysis. The formulations differ in how the convolution form of the viscoelastic constitutive equations are temporally discretized. A popular approach adopted by

Date: June 9, 2012.

Report Documentation Page

Form Approved
OMB No. 0704-0188

1. REPORT DATE	2. REPORT TYPE	3. DATES COVERED
09 JUN 2012		**00-00-2012 to 00-00-2012**

4. TITLE AND SUBTITLE	5a. CONTRACT NUMBER
A Nonlinear Finite Element Framework for Viscoelastic Beams Based on the High-Order Reddy Beam Theory	5b. GRANT NUMBER
	5c. PROGRAM ELEMENT NUMBER
6. AUTHOR(S)	5d. PROJECT NUMBER
	5e. TASK NUMBER
	5f. WORK UNIT NUMBER
7. PERFORMING ORGANIZATION NAME(S) AND ADDRESS(ES) **Texas A&M University,Department of Mechanical Engineering,College Station,TX,77843**	8. PERFORMING ORGANIZATION REPORT NUMBER
9. SPONSORING/MONITORING AGENCY NAME(S) AND ADDRESS(ES)	10. SPONSOR/MONITOR'S ACRONYM(S)
	11. SPONSOR/MONITOR'S REPORT NUMBER(S)

12. DISTRIBUTION/AVAILABILITY STATEMENT
Approved for public release; distribution unlimited

13. SUPPLEMENTARY NOTES
Journal of Engineering Materials and Technology, 2012 (in press)

14. ABSTRACT
A weak form Galerkin finite element model for the nonlinear quasi-static and fully transient analysis of initially straight viscoelastic beams is developed using the kinematic assumptions of the third-order Reddy beam theory. The formulation assumes linear viscoelastic material properties and is applicable to problems involving small strains and moderate rotations. The viscoelastic constitutive equations are efficiently discretized using the trapezoidal rule in conjunction with a two-point recurrence formula. Locking is avoided through the use of standard low order reduced integration elements as well through the employment of a family of elements constructed using high polynomial-order Lagrange and Hermite interpolation functions.

15. SUBJECT TERMS

16. SECURITY CLASSIFICATION OF:			17. LIMITATION OF ABSTRACT	18. NUMBER OF PAGES	19a. NAME OF RESPONSIBLE PERSON
a. REPORT **unclassified**	b. ABSTRACT **unclassified**	c. THIS PAGE **unclassified**	**Same as Report (SAR)**	**32**	

many researchers is to employ the Laplace transform method directly in the construction of the finite element equations [8, 1, 39]. In this approach, terms associated with the time domain, including the convolution integral, are transformed into variables associated with the Laplace space s. A successful numerical simulation therefore requires an efficient and accurate inversion of the solution in s space back to the time domain. Many of the key ideas are presented in work of Aköz and Kadioglu [1], wherein a Timoshenko beam element is developed using mixed variational principles. In their work, the finite element model requires numerical inversion from the Laplace-Carson domain back to the time domain. Temel et al. [39] utilized the Durbin's inverse Laplace transform method in their analysis of cylindrical helical rods (based on the Timoshenko beam hypotheses).

Additional numerical formulations for viscoelastic beams are based on the Fourier transform method [7], the anelastic displacement (ADN) procedure [40, 28] and the Golla-Hughes-McTavish (GHM) method [24, 25, 4, 3]. It has been noted that when the relaxation moduli are given as Prony series, the convolution form of linear viscoelastic constitutive equations may be equivalently expressed as a set of ordinary differential equations in terms of a collection of internal strain variables. Numerical discretization procedures exploiting this ODE form of the viscoelastic constitutive equations have been successfully adopted in the works of Johnson et al. [19] and Austin and Inman [2].

The formulations described above are restricted to a class of problems involving infinitesimal strains and small deflections. Among the finite element formulations appearing in the literature for nonlinear viscoelastic *shell* structures are the works of Kennedy [21], Oliveira and Creus [27] and Hammerand and Kapania [16]. More recently, Payette and Reddy [29] presented quasi-static finite element formulations for Euler-Bernoulli and Timoshenko beams that allow for loading scenarios that produce large transverse displacements, moderate rotations and small strains. This previous work may be viewed as a bridge between the formulations associated with either: (a) small strains or (b) fully finite deformations. In this prior work, the trapezoidal rule was employed in conjunction with a two-point recurrence formula for efficient temporal integration of the viscoelastic constitutive equations. The objective of the present paper is to extend the work of Payette and Reddy to create an efficient locking-free nonlinear finite element framework for the analysis of viscoelastic beam structures based on the high-order Reddy beam theory [30, 18, 41] for use in both quasi-static as well as fully dynamic analysis.

2. Kinematics of deformation

2.1. **The displacement field.** There are a variety of beam theories that have been successfully employed in the mechanical analysis of structural elements. Such theories are typically formulated in terms of truncated Taylor series expansions of the components of the displacement field with respect to the thickness coordinate. The most simple and commonly employed theories are the Euler-Bernoulli beam theory (EBT) and the Timoshenko beam theory (TBT). The major deficiency associated with the EBT is failure to account for deformations associated with shearing. The TBT relaxes the normality assumption of the EBT and admits a constant state of shear strain on a given cross-section. As a result, the TBT necessitates the use of shear correction coefficients in order to accurately predict transverse displacements. The third-order Reddy beam theory (RBT) was introduced to both account for the effects of shear strains and to also produce a parabolic variation of the shear strain through the thickness [30, 18, 41]. As a result, in the RBT there is no need to introduce shear correction coefficients.

Before presenting the displacement field associated with the RBT we first introduce some standard notation. We let $\mathcal{B} \subset \mathbb{R}^3$, an open and bounded set, denote the material or reference configuration of the beam. The material configuration may be expressed as $\mathcal{B} = \Omega \times A$, where $\Omega = (0, L)$ and L is the initial length of the beam. In addition the quantity A represents the beam's cross-sectional area. A typical material point belonging to $\mathcal{B}$ is denoted as $\mathbf{X} = (X, Y, Z)$. Likewise the spatial or current configuration of the beam is denoted by $\mathcal{B}_t$ and the associated points are expressed as $\mathbf{x} = (x, y, z)$. Points in the spatial configuration are related to points in the material configuration by the standard bijective mapping $\boldsymbol{\chi} : \mathcal{B} \times \mathbb{R} \to \mathcal{B}_t$. As a result $\mathbf{x} = \boldsymbol{\chi}(\mathbf{X}, t)$. The displacement field associated with the mapping may be expressed in the usual manner as $\mathbf{u}(\mathbf{X}, t) = \boldsymbol{\chi}(\mathbf{X}, t) - \mathbf{X}$.

In the present work, we constrain the displacement field to conform to the kinematic assumptions of the Reddy beam theory. The displacement field in the Reddy beam theory (for a beam with a rectangular cross section) is taken as

$$u(X, Y, Z, t) = u_0(X, t) + Z\phi_x(X, t) - Z^3 c_1 \left(\phi_x(X, t) + \frac{\partial w_0}{\partial X} \right) \tag{1a}$$

$$w(X, Y, Z, t) = w_0(X, t) \tag{1b}$$

where the X coordinate is taken along the beam length, the Z coordinate along the thickness direction of the beam, u_0 is the axial displacement of a point on the mid-plane $(X, 0, 0)$ of the

beam and w_0 represents the transverse deflection of the mid-plane. When the deformation is small the parameter $\phi_x(X,t)$ may be interpreted as the rotation of the transverse normal. The constant c_1 is equal to $c_1 = 4/(3h^2)$, where h is the height of the beam and b is the beam width. The displacement field of the Reddy beam theory suggests that a straight line perpendicular to the undeformed mid-plane becomes a cubic curve following deformation, as can be seen in Fig. 1.

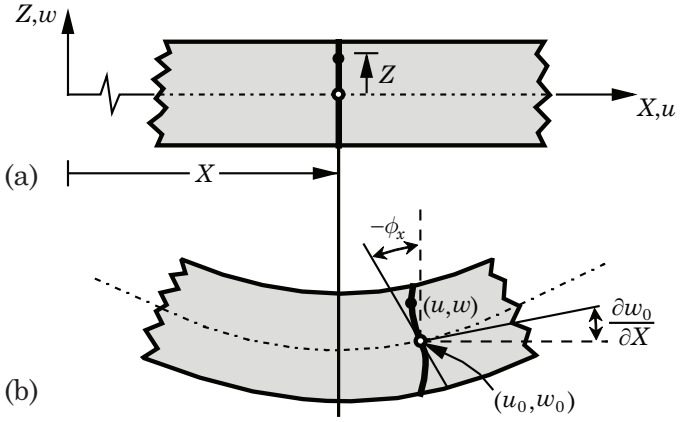

FIGURE 1. Deformation of a beam structure according to the third-order Reddy beam theory: (a) undeformed configuration and (b) deformed configuration.

2.2. **The effective strain tensor for the simplified theory.** In the mechanical analysis of deformable solids, it is necessary to employ stress and strain measures that are consistent with the deformations realized [34, 6]. When the deformations of the body are large, there are a variety of strain measures that may be employed. In our formulation we employ a total Lagrangian description of the deformation. In such analysis, the Green-Lagrange strain tensor $\mathbf{E}$ constitutes an appropriate measure of the strain at a point in the body. For the present analysis the non-zero components of $\mathbf{E}$ may be expressed as

$$E_{XX} = \frac{\partial u}{\partial X} + \frac{1}{2}\left[\left(\frac{\partial u}{\partial X}\right)^2 + \left(\frac{\partial w}{\partial X}\right)^2\right] \tag{2a}$$

$$E_{XZ} = \frac{1}{2}\left(\frac{\partial u}{\partial Z} + \frac{\partial w}{\partial X} + \frac{\partial u}{\partial X}\frac{\partial u}{\partial Z}\right) \tag{2b}$$

$$E_{ZZ} = \frac{1}{2}\left(\frac{\partial u}{\partial Z}\right)^2 \tag{2c}$$

In the present formulation we wish to develop a finite element framework that is applicable under loading conditions that produce large transverse displacements, moderate rotations

$(10-15^{\circ})$ and small strains [32]. Under such conditions it is possible to neglect the underlined terms in the above definition of the Green-Lagrange strain tensor. Consequently, we employ a reduced form of the Green-Lagrange strain tensor, denoted by ε, whose non-zero components may be expressed as

$$\varepsilon_{xx} = \frac{\partial u_0}{\partial x} + \frac{1}{2}\left(\frac{\partial w_0}{\partial x}\right)^2 + z\frac{\partial \phi_x}{\partial x} - z^3 c_1 \left(\frac{\partial \phi_x}{\partial x} + \frac{\partial^2 w_0}{\partial x^2}\right) \tag{3a}$$

$$\gamma_{xz} = 2\varepsilon_{xz} = \left(1 - c_2 z^2\right)\left(\phi_x + \frac{\partial w_0}{\partial x}\right) \tag{3b}$$

where $c_2 = 3c_1$. The strain components associated with the linearized strain tensor ε are commonly called the the von Kármán strain components. For a comparison of numerical results obtained using the above simplified theory with the full nonlinear theory for elastic structures, we refer to the work of Başar *et al.* [5]. It is important to note that the material coordinates appearing in the definition of the reduced strain components and throughout the remainder of this paper are denoted as (x, y, z) as a reminder that the present formulation is applicable to small strains and moderate rotations, and is therefore a linearization of the more general finite deformation theory.

2.3. **Linear viscoelastic constitutive equations.** For linear viscoelastic materials, the constitutive equations relating the components of the second Piola Kirchhoff stress tensor $\mathbf{S}$ to the Green-Lagrange strain $\mathbf{E}$ may be expressed in terms of the following set of integral equations

$$\mathbf{S}(t) = \mathbb{C}(0) : \mathbf{E}(t) + \int_0^t \dot{\mathbb{C}}(t-s) : \mathbf{E}(s) ds \tag{4}$$

where $\dot{\mathbb{C}}(t-s) \equiv d\mathbb{C}(t-s)/d(t-s)$ and $\mathbb{C}(t)$ is the fourth-order viscoelasticity relaxation tensor. In the present analysis the above expression reduces to

$$\sigma_{xx}(\mathbf{x}, t) = E(0)\varepsilon_{xx}(\mathbf{x}, t) + \int_0^t \dot{E}(t-s)\varepsilon_{xx}(\mathbf{x}, s) ds \tag{5a}$$

$$\sigma_{xz}(\mathbf{x}, t) = G(0)\gamma_{xz}(\mathbf{x}, t) + \int_0^t \dot{G}(t-s)\gamma_{xz}(\mathbf{x}, s) ds \tag{5b}$$

where σ_{xx} and σ_{xz} are the nonzero components of second Piola Kirchhoff stress tensor used in the present simplified formulation. The quantities $E(t)$ and $G(t)$ are the relaxation moduli. The specific forms of $E(t)$ and $G(t)$ will depend upon the material model employed. For the present analysis we assume that these relaxation functions can be expanded as Prony series

of order NPS as

$$E(t) = E_0 + \sum_{l=1}^{\text{NPS}} \bar{E}_l(t), \qquad G(t) = G_0 + \sum_{l=1}^{\text{NPS}} \bar{G}_l(t) \tag{6}$$

where $\bar{E}_l(t)$ and $\bar{G}_l(t)$ have been defined as (following the generalized Maxwell model)

$$\bar{E}_l(t) = E_l e^{-t/\tau_l^E}, \qquad \bar{G}_l(t) = G_l e^{-t/\tau_l^G} \tag{7}$$

It is important to emphasize that the Prony series representation of the viscoelastic relaxation moduli is critical for the implementation of efficient temporal numerical integration algorithms of the integral type viscoelastic constitutive equations considered in this paper. We note in passing that effective temporal integration algorithms for alternative classes of viscoelastic constitutive equations, such as fractional derivative models, have also been adopted in the literature (see for example Refs. [10, 11, 12, 15, 42]).

3. Weak form Galerkin finite element model

3.1. **Weak formulation.** The weak form Galerkin finite element model of the third order Reddy beam theory may be developed by applying the principle of virtual displacements to a typical beam as viewed in the reference configuration. The dynamic form of the virtual work statement may therefore be expressed as

$$\begin{aligned}
\delta\mathcal{W} &= -\delta\mathcal{K} + \delta\mathcal{W}_{\text{I}} + \delta\mathcal{W}_{\text{E}} \\
&= \int_{\mathcal{B}} \big(\delta\mathbf{u}\cdot\rho_0\ddot{\mathbf{u}} + \delta\mathbf{E} : \mathbf{S} - \delta\mathbf{u}\cdot\rho_0\mathbf{b}\big) dV - \int_{\Gamma_\sigma} \delta\mathbf{u}\cdot\mathbf{t}_0 dS \\
&\cong \int_0^L \int_A \big(\delta\mathbf{u}\cdot\rho_0\ddot{\mathbf{u}} + \delta\varepsilon : \sigma - \delta\mathbf{u}\cdot\rho_0\mathbf{b}\big) dA dx - \int_{\Gamma_\sigma} \delta\mathbf{u}\cdot\mathbf{t}_0 dS \equiv 0
\end{aligned} \tag{8}$$

where $\delta\mathcal{K}$ is the virtual kinetic energy, $\delta\mathcal{W}_{\text{I}}$ is the internal virtual work and $\delta\mathcal{W}_{\text{E}}$ is the external virtual work. The additional quantities ρ_0, $\mathbf{b}$ and $\mathbf{t}_0$ are the density, body force and traction vector, respectively. The above expression constitutes the weak form of the classical Euler-Lagrange equations of motion of a continuous body.

In the finite element method we assume that the material domain $\bar{\Omega} = [0, L]$ is partitioned into a set of NE non-overlapping sub-domains $\bar{\Omega}^e = [x_a^e, x_b^e]$, called finite elements, such that $\bar{\Omega} = \bigcup_{e=1}^{\text{NE}} \bar{\Omega}^e$. The resulting variational problem associated with the weak formulation of the Reddy beam equations may therefore be expressed as follows: find $(u_0, w_0, \phi_x) \in \mathcal{V}$ such

that for all $(\delta u_0, \delta w_0, \delta\phi_x) \in \mathcal{X}$ the following expressions hold within each element:

$$0 = \int_{x_a}^{x_b} \left(I_0 \delta u_0 \ddot{u}_0 + \frac{\partial \delta u_0}{\partial x} N_{xx} - \delta u_0 f \right) dx - \delta u_0(x_a) Q_1 - \delta u_0(x_b) Q_5 \tag{9a}$$

$$\begin{aligned} 0 = \int_{x_a}^{x_b} \Bigg[& I_0 \delta w_0 \ddot{w}_0 + \frac{\partial \delta w_0}{\partial x} \left(c_1^2 I_6 \frac{\partial \ddot{w}_0}{\partial x} - J_4 \ddot{\phi}_x \right) + \frac{\partial \delta w_0}{\partial x} \left(\frac{\partial w_0}{\partial x} N_{xx} + Q_x - c_2 R_x \right) \\ & - \frac{\partial^2 \delta w_0}{\partial x^2} c_1 P_{xx} - \delta w_0 q \Bigg] dx - Q_2 \delta w_0(x_a) - Q_6 \delta w_0(x_b) - Q_3 \left(-\frac{\partial \delta w_0}{\partial x} \right) \Bigg|_{x=x_a} \\ & - Q_7 \left(-\frac{\partial \delta w_0}{\partial x} \right) \Bigg|_{x=x_b} \end{aligned} \tag{9b}$$

$$\begin{aligned} 0 = \int_{x_a}^{x_b} & \left[\delta\phi_x \left(-J_4 \frac{\partial \ddot{w}_0}{\partial x} + K_2 \ddot{\phi}_x \right) + \delta\phi_x (Q_x - c_2 R_x) + \frac{\partial \delta\phi_x}{\partial x} (M_{xx} - c_1 P_{xx}) \right] dx \\ & - Q_4 \delta\phi_x(x_a) - Q_8 \delta\phi_x(x_b) \end{aligned} \tag{9c}$$

where $\mathcal{V}$ and $\mathcal{X}$ are appropriate function spaces. It is important to note that in the finite element implementation, w_0 must be approximated using Hermite polynomials. Consequently, the nodal degrees of freedom of the resulting finite element model will contain not only w_0 but also its derivative. For the sake of brevity we have omitted the superscript e from quantities appearing in the above equations (e.g., x_a and x_b) and throughout the remainder of this work. The quantities f and q appearing above are the distributed axial and transverse loads respectively. We have also introduced the following constants

$$I_i = \rho_0 D_i = \rho_0 \int_A z^i dA, \qquad J_4 = c_1(I_4 - c_1 I_6), \qquad K_2 = I_2 - 2c_1 I_4 + c_1^2 I_6 \tag{10}$$

The internal stress resultants N_{xx}, M_{xx}, P_{xx}, Q_x and R_x are defined as

$$\left\{ \begin{array}{c} N_{xx} \\ M_{xx} \\ P_{xx} \end{array} \right\} = \int_A \left\{ \begin{array}{c} 1 \\ z \\ z^3 \end{array} \right\} \sigma_{xx} dA, \qquad \left\{ \begin{array}{c} Q_x \\ R_x \end{array} \right\} = \int_A \left\{ \begin{array}{c} 1 \\ z^2 \end{array} \right\} \sigma_{xz} dA \tag{11}$$

and can be expressed in terms of the generalized displacements (u_0, w_0, ϕ_x) through the use of the viscoelastic constitutive equations. The quantities N_{xx}, M_{xx} and Q_x are the internal axial force, bending moment and shear force. In addition, P_{xx} and R_x are higher order stress resultants that arise in the third order beam theory due to the cubic expansion of the axial displacement field. The quantities Q_j (j=1,..,8) are the externally applied generalized nodal forces.

3.2. **Semi-discrete finite element equations.** In this subsection we develop the semi-discrete finite element equations associated with the third order Reddy beam theory. Within a typical finite element the dependent variables may be adequately approximated using the following interpolation formulas

$$\begin{aligned} u_0(x,t) &= \sum_{j=1}^{n} \Delta_j^{(1)}(t)\psi_j^{(1)}(x), \quad w_0(x,t) = \sum_{j=1}^{2n} \Delta_j^{(2)}(t)\psi_j^{(2)}(x) \\ \phi_x(x,t) &= \sum_{j=1}^{n} \Delta_j^{(3)}(t)\psi_j^{(1)}(x) \end{aligned} \tag{12}$$

where a space-time decoupled formulation has been adopted and n represents the number of nodes per element. In the finite element method, the geometry of each element is characterized using the standard isoparametric mapping from the master element $\hat{\Omega}^e = [-1, +1]$ to the physical element $\bar{\Omega}^e = [x_a^e, x_b^e]$. The quantities $\Delta_j^{(1)}(t)$, $\Delta_j^{(2)}(t)$ and $\Delta_j^{(3)}(t)$ are the generalized displacements at the element nodes. In addition $\psi_j^{(1)}(x)$ and $\psi_j^{(2)}(x)$ are the $(n-1)$th-order Lagrange and $(2n-1)$th-order Hermite interpolation functions respectively. Inserting Equation Eq. (12) into Eqs. (9a) through (9c) results in the semi-discrete finite element equations for the RBT. The resulting set of equations for a typical element may be expressed as at the current time t as

$$[M^e]\{\ddot{\Delta}^e\} + [K^e]\{\Delta^e\} + \int_0^t \{\Lambda^e(t,s)\}ds = \{F^e\} \tag{13}$$

The element level equations may be partitioned into the following equivalent set of expressions

$$[M^{\alpha\beta}]\{\ddot{\Delta}^{(\beta)}\} + [K^{\alpha\beta}]\{\Delta^{(\beta)}\} + \int_0^t \{\Lambda^{(\alpha)}(t,s)\}ds = \{F^{(\alpha)}\} \tag{14}$$

where α and β range from 1 to 3 and Einstein's summation convention is implied over β. Expressions for determining the components of the partitioned element coefficient matrices and vectors are given explicitly in Appendix A.

3.3. **Fully-discrete finite element equations.** In this subsection we develop the fully discretized finite element equations for the Reddy beam theory. We begin by partitioning the time interval $[0, \tau] \subset \mathbb{R}$ of interest in the analysis, where $\tau > 0$, into a set of N non-overlapping subintervals such that $[0, \tau] = \bigcup_{k=1}^{N} \mathcal{I}_k$, and $\mathcal{I}_k = [t_k, t_{k+1}]$. The solution may then be obtained incrementally by solving an initial value problem within each subinterval $\mathcal{I}_k$, where we assume that the solution is known at $t = t_k$. Within each subregion it is

therefore necessary to introduce approximations for both the temporal derivatives of the generalized displacements (resulting from the inertia terms) as well as the convolution integrals (resulting from the viscoelastic constitutive model of the material). Since temporal integration of the inertia terms is relatively straightforward, we restrict the current discussion to discretization of the quasi-static form of the semi-discrete finite element equations only. In this work, we approximate the convolution integrals using the trapezoidal rule within each time subinterval. We further introduce a two-point recurrence formula, associated with a set of history variables that are evaluated at the quadrature points, that is utilized to effectively advance the numerical solution from one time step to the next such that data history is only necessary from the immediate previous time step. Although not entirely the same, the adopted procedure has its roots in many of the key ideas presented in the pioneering work of Taylor et al. [38], where the finite element method was first employed to solve problems in viscoelasticity using algorithms based on recurrence formulas.

We assume, without loss of generality, that the quasi-static semi-discrete finite element equations have been successfully integrated temporally up until $t = t_k$. Our goal, therefore, is to numerically integrate the finite element equations over the subinterval $\mathcal{I}_k$ to obtain the solution for the generalized displacements at $t = t_{k+1}$. Before proceeding we must emphasize that all subsequent discussions regarding efficient recurrence based temporal integration strategies rely on the following multiplicative decompositions of the Prony series terms appearing in the definition of the relaxation moduli [37]

$$\dot{\bar{E}}_l(t_{k+1} - s) = e^{-\Delta t_{k+1}/\tau_l^E}\, \dot{\bar{E}}_l(t_k - s), \qquad \dot{\bar{G}}_l(t_{k+1} - s) = e^{-\Delta t_{k+1}/\tau_l^G}\, \dot{\bar{G}}_l(t_k - s) \tag{15}$$

where $\Delta t_{k+1} = t_{k+1} - t_k$ is the time step associated with subinterval $\mathcal{I}_k$. With the above formulas in mind, we note that the components of $\Lambda_i^\alpha(t_{k+1}, s)$ may be conveniently expressed as

$$\Lambda_i^\alpha(t_{k+1}, s) = \sum_{j=1}^{n_\alpha} {}^j\bar{\Lambda}_i^\alpha(t_{k+1}, s) \tag{16}$$

where $n_1 = 1$, $n_2 = 3$ and $n_3 = 2$. The components ${}^j\bar{\Lambda}_i^\alpha(t_{k+1}, s)$ can be decomposed multiplicatively using the following general formula

$${}^j\bar{\Lambda}_i^\alpha(t_{k+1}, s) = \sum_{m=1}^{\text{NGP}} \sum_{l=1}^{\text{NPS}} {}_m^j\chi_i^\alpha(t_{k+1})\, {}_l^j\beta^\alpha(\Delta t_{k+1})\, {}_{lm}^j\kappa^\alpha(t_k, s) W_m \tag{17}$$

In the above expression we have employed the Gauss-Legendre quadrature rule in evaluation of all spatial integrals (resulting in summation over m). The quantity W_m represents the mth quadrature weight associated with the Gauss-Legendre quadrature rule. Summation over l is due to the Prony series representation of the relaxation moduli. The multiplicative decomposition of each ${}^{j}\bar{\Lambda}_i^{\alpha}(t_{k+1}, s)$ is essential for the recurrence based integration strategy. The components of ${}^{j}_{m}\chi_i^{\alpha}(t_{k+1})$ are used to store the discrete finite element test functions as well as any nonlinear quantities associated with the first variation of the simplified Green-Lagrange strain tensor. In the present formulation the components of ${}^{j}_{m}\chi_i^{\alpha}(t_{k+1})$ are defined as

$$
\begin{aligned}
{}^{1}_{m}\chi_i^{1}(t_{k+1}) &= \frac{d\psi_i^{(1)}(x_m)}{dx} && \text{(18a)}\\
{}^{1}_{m}\chi_i^{2}(t_{k+1}) &= \frac{\partial w_0(x_m, t_{k+1})}{\partial x}\frac{d\psi_i^{(2)}(x_m)}{dx} && \text{(18b)}\\
{}^{2}_{m}\chi_i^{2}(t_{k+1}) &= \frac{d^2\psi_i^{(2)}(x_m)}{dx^2} && \text{(18c)}\\
{}^{3}_{m}\chi_i^{2}(t_{k+1}) &= \frac{d\psi_i^{(2)}(x_m)}{dx} && \text{(18d)}\\
{}^{1}_{m}\chi_i^{3}(t_{k+1}) &= {}^{1}_{m}\chi_i^{1}(t_{k+1}) && \text{(18e)}\\
{}^{2}_{m}\chi_i^{3}(t_{k+1}) &= \psi_i^{(1)}(x_m) && \text{(18f)}
\end{aligned}
$$

In the above expression, x_m represents the value of x as evaluated at the mth quadrature point of a given finite element. The isoparametric mapping $\hat{\Omega}^e \rightleftarrows \bar{\Omega}^e$ used to characterize the geometry of each element allows for simple evaluation of such expressions. The components of ${}^{j}_{l}\beta^{\alpha}(\Delta t_{k+1})$ are defined as

$$
\begin{aligned}
&{}^{1}_{l}\beta^{1}(\Delta t_{k+1}) = {}^{1}_{l}\beta^{2}(\Delta t_{k+1}) = {}^{2}_{l}\beta^{2}(\Delta t_{k+1}) = {}^{1}_{l}\beta^{3}(\Delta t_{k+1}) = e^{-\Delta t_{k+1}/\tau_l^E}\\
&{}^{3}_{l}\beta^{2}(\Delta t_{k+1}) = {}^{2}_{l}\beta^{3}(\Delta t_{k+1}) = e^{-\Delta t_{k+1}/\tau_l^G}
\end{aligned}
\qquad \text{(19)}
$$

Likewise, the components of ${}^{j}_{lm}\kappa^{\alpha}(t_k, s)$ may be determined using the following formulas

$$
\begin{aligned}
{}^{1}_{lm}\kappa^{1}(t_k, s) &= \dot{\bar{E}}_l(t_k - s)D_0\left[\frac{\partial u_0(x_m, s)}{\partial x} + \frac{1}{2}\left(\frac{\partial w_0(x_m, s)}{\partial x}\right)^2\right] && \text{(20a)}\\
{}^{1}_{lm}\kappa^{2}(t_k, s) &= {}^{1}_{lm}\kappa^{1}(t_k, s) && \text{(20b)}\\
{}^{2}_{lm}\kappa^{2}(t_k, s) &= \dot{\bar{E}}_l(t_k - s)\left(c_1^2 D_6\frac{\partial^2 w_0(x_m, s)}{\partial x^2} - L_4\frac{\partial \phi_x(x_m, s)}{\partial x}\right) && \text{(20c)}
\end{aligned}
$$

$$ {}^{3}_{lm}\kappa^{2}(t_k,s) = \dot{\bar{G}}_l(t_k-s)\hat{A}_s\left(\frac{\partial w_0(x_m,s)}{\partial x}+\phi_x(x_m,s)\right) \tag{20d} $$

$$ {}^{1}_{lm}\kappa^{3}(t_k,s) = \dot{\bar{E}}_l(t_k-s)\left(M_2\frac{\partial \phi_x(x_m,s)}{\partial x}-L_4\frac{\partial^2 w_0(x_m,s)}{\partial x^2}\right) \tag{20e} $$

$$ {}^{2}_{lm}\kappa^{3}(t_k,s) = {}^{3}_{lm}\kappa^{2}(t_k,s) \tag{20f} $$

It is important to note that the components of ${}^{j}_{lm}\kappa^{\alpha}(t_k,s)$ have been defined such that the following multiplicative recurrence formulas holds

$$ {}^{j}_{lm}\kappa^{\alpha}(t_{k+1},s) = {}^{j}_{l}\beta^{\alpha}(\Delta t_{k+1}){}^{j}_{lm}\kappa^{\alpha}(t_k,s) \tag{21} $$

The above expressions are admissible on account of the assumption that the relaxation parameters are expressed in terms of Prony series.

We assume that at $t=t_k$ the components of the following expression are known

$$ \int_0^{t_k} {}^{j}\bar{\Lambda}^{\alpha}_{i}(t_k,s)ds = \sum_{m=1}^{\text{NGP}}\sum_{l=1}^{\text{NPS}} {}^{j}_{m}\chi^{\alpha}_{i}(t_k){}^{j}_{lm}X^{\alpha}(t_k)W_m \tag{22} $$

where ${}^{j}_{lm}X^{\alpha}(t_k)$ is a set of history variables (stored at the quadrature points of each element) that are of the form

$$ {}^{j}_{lm}X^{\alpha}(t_k) = \int_0^{t_k} {}^{j}_{lm}\kappa^{\alpha}(t_k,s)ds \tag{23} $$

We note that ${}^{j}_{lm}X^{\alpha}(0)=0$. At $t=t_k$ the above history variables are known and there is no need to explicitly evaluate the expression appearing on the right hand side of Eq. (23). At the subsequent time step $t=t_{k+1}$ Eq. (22) may be written as

$$ \begin{aligned} \int_0^{t_{k+1}} {}^{j}\bar{\Lambda}^{\alpha}_{i}(t_{k+1},s)ds &= \int_0^{t_k} {}^{j}\bar{\Lambda}^{\alpha}_{i}(t_{k+1},s)ds + \int_{t_k}^{t_{k+1}} {}^{j}\bar{\Lambda}^{\alpha}_{i}(t_{k+1},s)ds \\ &= \sum_{m=1}^{\text{NGP}}\sum_{l=1}^{\text{NPS}} {}^{j}_{m}\chi^{\alpha}_{i}(t_{k+1}){}^{j}_{l}\beta^{\alpha}(\Delta t_{k+1}){}^{j}_{lm}X^{\alpha}(t_k)W_m \\ &\quad + \int_{t_k}^{t_{k+1}} {}^{j}\bar{\Lambda}^{\alpha}_{i}(t_{k+1},s)ds \end{aligned} \tag{24} $$

It is important to note that we have expressed the first integral on the right hand side of the above equation in terms of ${}^{j}_{lm}X^{\alpha}(t_k)$ (which is known from the previous time step). To integrate the remaining expression in Eq. (24) over the subinterval $\mathcal{I}_k$ we employ the

trapezoidal rule which may be expressed as

$$\begin{aligned}\int_{t_k}^{t_{k+1}} {}^{j}\bar{\Lambda}_i^{\alpha}(t_{k+1},s)ds &\cong \frac{\Delta t_{k+1}}{2}\left[{}^{j}\bar{\Lambda}_i^{\alpha}(t_{k+1},t_k)+{}^{j}\bar{\Lambda}_i^{\alpha}(t_{k+1},t_{k+1})\right]\\ &= \frac{\Delta t_{k+1}}{2}\sum_{m=1}^{\text{NGP}}\sum_{l=1}^{\text{NPS}} {}_{m}^{j}\chi_i^{\alpha}(t_{k+1})_{l}^{j}\beta^{\alpha}(\Delta t_{k+1})\left[{}_{lm}^{j}\kappa^{\alpha}(t_k,t_k)\right.\\ &\quad \left.+{}_{lm}^{j}\kappa^{\alpha}(t_k,t_{k+1})\right]W_m\end{aligned} \tag{25}$$

As a result, Eq. (24) can be written in the following simplified form

$$\int_{0}^{t_{k+1}} {}^{j}\bar{\Lambda}_i^{\alpha}(t_{k+1},s)ds = \sum_{m=1}^{\text{NGP}}\sum_{l=1}^{\text{NPS}} {}_{m}^{j}\chi_i^{\alpha}(t_{k+1})_{lm}^{j}X^{\alpha}(t_{k+1})W_m \tag{26}$$

where

$$\begin{aligned}{}_{lm}^{j}X^{\alpha}(t_{k+1}) &= \frac{\Delta t_{k+1}}{2}{}_{l}^{j}\beta^{\alpha}(\Delta t_{k+1})\left[{}_{lm}^{j}\kappa^{\alpha}(t_k,t_k)+{}_{lm}^{j}\kappa^{\alpha}(t_k,t_{k+1})\right]\\ &\quad +{}_{l}^{j}\beta^{\alpha}(\Delta t_{k+1})_{lm}^{j}X^{\alpha}\left(t_k\right)\end{aligned} \tag{27}$$

As a result, in Eq. (26) we have developed a general expression for integrating the viscoelastic terms up to any discrete instance in time. The expression relies on a recurrence relationship defined in terms of the set of history variables ${}_{lm}^{j}X^{\alpha}(t_{k+1})$. These variables must be stored in memory at the immediate previous time step and may be updated to the subsequent time step in accordance with the procedure outlined in Eq. (27). The history variables are expressed explicitly in Appendix B. It is now possible to express the fully discretized finite element equations at the current time step as

$$[\bar{K}^e]_{k+1}\{\Delta^e\}_{k+1} = \{F^e\}_{k+1} - \{\tilde{Q}^e\}_{k+1} \tag{28}$$

where each of the components in the above equation are given in Appendix B.

3.4. **Iterative solution of nonlinear equations using Newton's method.** The fully discretized finite element equations are nonlinear due to the use of the von Kármán strain components in the definition of the effective strain tensor ε. In our work, we adopt the Newton procedure in the iterative solution of the nonlinear finite element equations. The resulting linearized finite element equations are of the form

$$[T^e]_{k+1}^{(r)}\{\delta\Delta^e\}_{k+1}^{(r+1)} = -([\bar{K}^e]_{k+1}^{(r)}\{\Delta^e\}_{k+1}^{(r)} - \{F^e\}_{k+1}^{(r)} + \{\tilde{Q}^e\}_{k+1}^{(r)}) \tag{29}$$

where $\{\delta\Delta^e\}_{k+1}^{(r+1)}$ represents the incremental solution at the $(r+1)$th nonlinear iteration. The total global solution at the $(r+1)$th iteration is obtained as

$$\{\Delta\}_{k+1}^{(r+1)} = \{\delta\Delta\}_{k+1}^{(r+1)} + \{\Delta\}_{k+1}^{(r)} \tag{30}$$

The element tangent stiffness coefficient matrix $[T^e]_{k+1}^{(r)}$ appearing in the Newton linearization of the finite element equations may be expressed (using Einstein's summation convention over n) as

$$T_{ij}^e = \bar{K}_{ij}^e + \frac{\partial \bar{K}_{in}^e}{\partial \Delta_j^e}\Delta_n^e + \frac{\partial \tilde{Q}_i^e}{\partial \Delta_j^e} \tag{31}$$

All quantities comprising the tangent stiffness matrix are formulated using the solution from the rth iteration. The partial derivatives are taken with respect to the solution at the current time step. Formulas for evaluating the components of the element tangent stiffness coefficient matrix are given in Appendix C.

3.5. **Finite element interpolation of dependent variables.** It is well-known that low-order finite elements for beams are prone to locking [34, 31, 33] when quadrature rules are employed that result in exact integration of the element coefficient matrices and force vectors. To circumvent the locking phenomena, we consider two philosophically dissimilar numerical procedures. In the first approach, we employ the lowest order element admissible in the formulation (i.e., a two-noded element). Selective full and one point Gauss-Legendre quadrature rules are applied; where reduced integration techniques are employed on all nonlinear expressions associated with the finite element model. This element is denoted as an RBT-2-R element (meaning a two-noded reduced integration RBT element). It is worth noting that this element requires a splitting of the history variables into subsets associated with the full and reduced quadrature points. In the second approach, we construct the Reddy beam finite elements using high-polynomial order expansions of the dependent variables, by systematically increasing the number of nodes per finite element. In this approach, the same quadrature formulas may be employed in the evaluation of all expressions appearing in the coefficient matrices and force vectors of the finite element model. The resulting elements are denoted in this work as RBT-n elements, where n represents the number of nodes per element.

In the proposed high-order finite element formulation, we employ an unequal spacing of the nodes within each element. We define the nodal points, within the master element

$\hat{\Omega}^e = [-1, +1]$, in terms of the roots of the following expression

$$(\xi - 1)(\xi + 1)L'_p(\xi) = 0 \qquad \text{in } \hat{\Omega}^e \tag{32}$$

where $L_p(\xi)$ is the Legendre polynomial of order p [17] and $n = p+1$ represents the number of nodes per element. As a result, the quantities ξ_i, where $i = 1, .., n$, are the nodal points associated with $\hat{\Omega}^e$. In our formulation we construct the high-order Lagrange interpolation functions in accordance with the following expression

$$\psi_i^{(1)}(\xi) = \frac{(\xi - 1)(\xi + 1)L'_p(\xi)}{p(p+1)L_p(\xi_i)(\xi - \xi_i)} \qquad \text{in } \hat{\Omega}^e \tag{33}$$

The above interpolation functions are often called spectral nodal interpolation functions in the literature [20]. The high-order Hermite interpolation functions $\hat{\psi}_i^{(2)}$ associated with the master element $\hat{\Omega}^e$ may be calculated as

$$\hat{\psi}_i^{(2)}(\xi) = \sum_{j=1}^{2n} c_i^{j-1} \xi^{j-1} \tag{34}$$

The coefficients c_i^{j-1} appearing in the above expression may be determined by imposing the following compatibility conditions on the interpolation functions

$$\hat{\psi}_{2i-1}^{(2)}(\xi_j) = -\frac{d\hat{\psi}_{2i}^{(2)}}{d\xi}\bigg|_{\xi=\xi_j} = \delta_{ij}, \qquad \frac{d\hat{\psi}_{2i-1}^{(2)}}{d\xi}\bigg|_{\xi=\xi_j} = \hat{\psi}_{2i}^{(2)}(\xi_j) = 0 \tag{35}$$

where i and j both range from 1 to n. The Hermite interpolation functions $\psi_i^{(2)}$ associated with the physical element $\bar{\Omega}^e$ may be determined as

$$\psi_{2i-1}^{(2)}(\xi) = \hat{\psi}_{2i-1}^{(2)}(\xi), \qquad \psi_{2i}^{(2)}(\xi) = J^e \hat{\psi}_{2i}^{(2)}(\xi) \tag{36}$$

where J^e is the Jacobian of the element coordinate transformation $\hat{\Omega}^e \rightleftarrows \bar{\Omega}^e$. The above formulas may be utilized to generate high-order Lagrange and Hermite interpolation functions for any number of nodes per element. The standard lowest order two-noded element may be obtained as a special case. The interpolation functions associated with a six-node RBT finite element are shown in Fig. 2.

4. Numerical examples

In this section, numerical results are presented and tabulated for the mechanical response of viscoelastic beam structures obtained using the proposed finite element formulation for

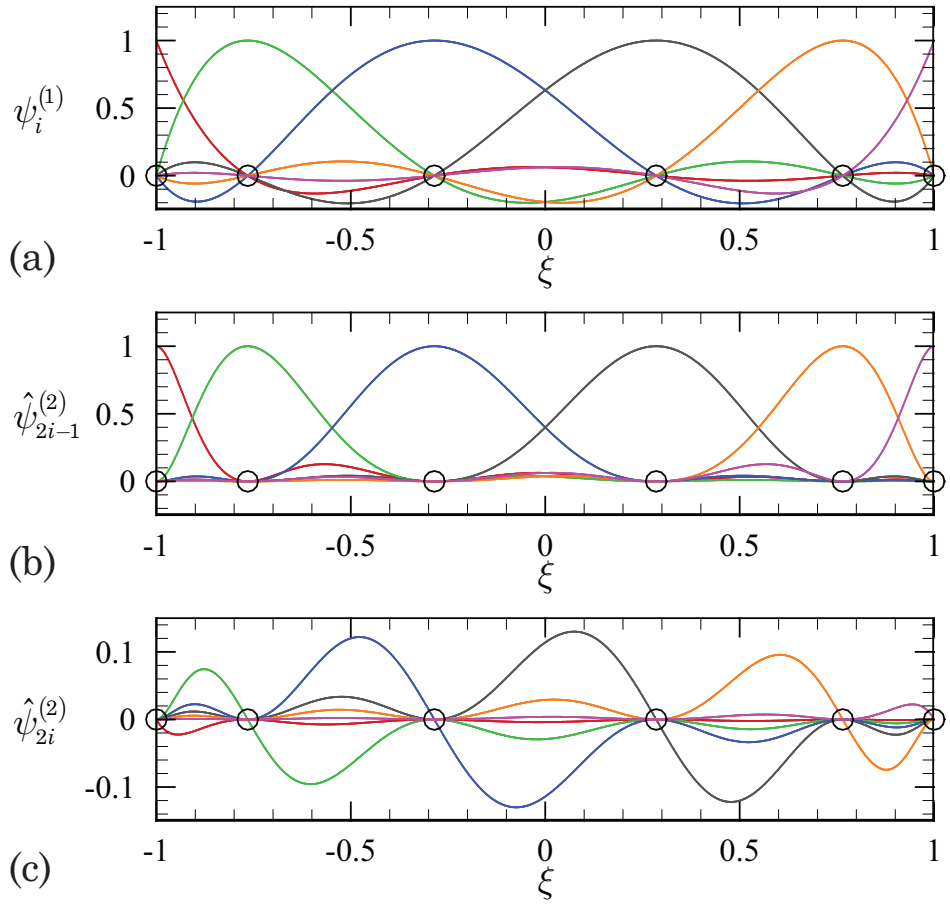

FIGURE 2. Interpolation functions for a high-order RBT finite element where $n = 6$ and $i = 1, .., n$: (a) Lagrange interpolation functions $\psi_i^{(1)}$, (b) Hermite interpolation functions $\hat{\psi}_{2i-1}^{(2)}$ and (c) Hermite interpolation functions $\hat{\psi}_{2i}^{(2)}$.

the third-order Reddy beam theory. The results presented in this section have been obtained using the Newton solution procedure described in the previous section. Nonlinear convergence is declared at time t_{k+1} once the Euclidean norm of the normalized difference between the nonlinear iterative solution increments (i.e., $||\{\Delta\}_{k+1}^{(r+1)} - \{\Delta\}_{k+1}^{(r)}||/||\{\Delta\}_{k+1}^{(r+1)}||$), is less than 10^{-6}.

The material model utilized in the quasi-static numerical studies is based upon the experimental results tabulated by Lai and Bakker [23] for a glassy amorphous polymer material (PMMA). The Prony series parameters for the viscoelastic relaxation modulus given in Table 1 were calculated by Payette and Reddy [29] from the published compliance parameters [23]. As in the work of Chen [8] and Payette and Reddy [29], we assume that Poisson's ratio is

time invariant. As a result, the shear relaxation moduli is given as

$$G(t) = \frac{E(t)}{2(1+\nu)} \tag{37}$$

where Poisson's ratio is taken to be $\nu = 0.40$ [22].

TABLE 1. Viscoelastic relaxation parameters for a PMMA.

E_0	205.7818 ksi		
E_1	43.1773 ksi	τ_1^E	9.1955×10^{-1} sec.
E_2	9.2291 ksi	τ_2^E	9.8120×10^{0} sec.
E_3	22.9546 ksi	τ_3^E	9.5268×10^{1} sec.
E_4	26.2647 ksi	τ_4^E	9.4318×10^{2} sec.
E_5	34.6298 ksi	τ_5^E	9.2066×10^{3} sec.
E_6	40.3221 ksi	τ_6^E	8.9974×10^{4} sec.
E_7	47.5275 ksi	τ_7^E	8.6852×10^{5} sec.
E_8	46.8108 ksi	τ_8^E	8.5143×10^{6} sec.
E_9	58.6945 ksi	τ_9^E	7.7396×10^{7} sec.

4.1. **Quasi-static deflection of various thin beams under uniform loading.** In this first example we consider a viscoelastic beam of length $L = 100$ in. and cross section 1 in. $\times$ 1 in. At $t = 0$ sec. the beam is subjected to a uniform vertically distributed load $q_0 = 0.25$ lb_f/in. Due to symmetry about $x = L/2$, it is only necessary to model half of the physical domain. To assess the performance of various finite element discretizations in circumventing the locking phenomena, we consider the following three sets of boundary conditions:

(1) Hinged at both ends

$$w_0(0,t) = u_0(L/2,t) = \frac{\partial w_0}{\partial x}(L/2,t) = \phi_x(L/2,t) = 0 \tag{38}$$

(2) Pinned at both ends

$$u_0(0,t) = w_0(0,t) = u_0(L/2,t) = \frac{\partial w_0}{\partial x}(L/2,t) = \phi_x(L/2,t) = 0 \tag{39}$$

(3) Clamped at both ends

$$\begin{aligned} u_0(0,t) = w_0(0,t) = \frac{\partial w_0}{\partial x}(0,t) = \phi_x(0,t) = 0 \\ u_0(L/2,t) = \frac{\partial w_0}{\partial x}(L/2,t) = \phi_x(L/2,t) = 0 \end{aligned} \tag{40}$$

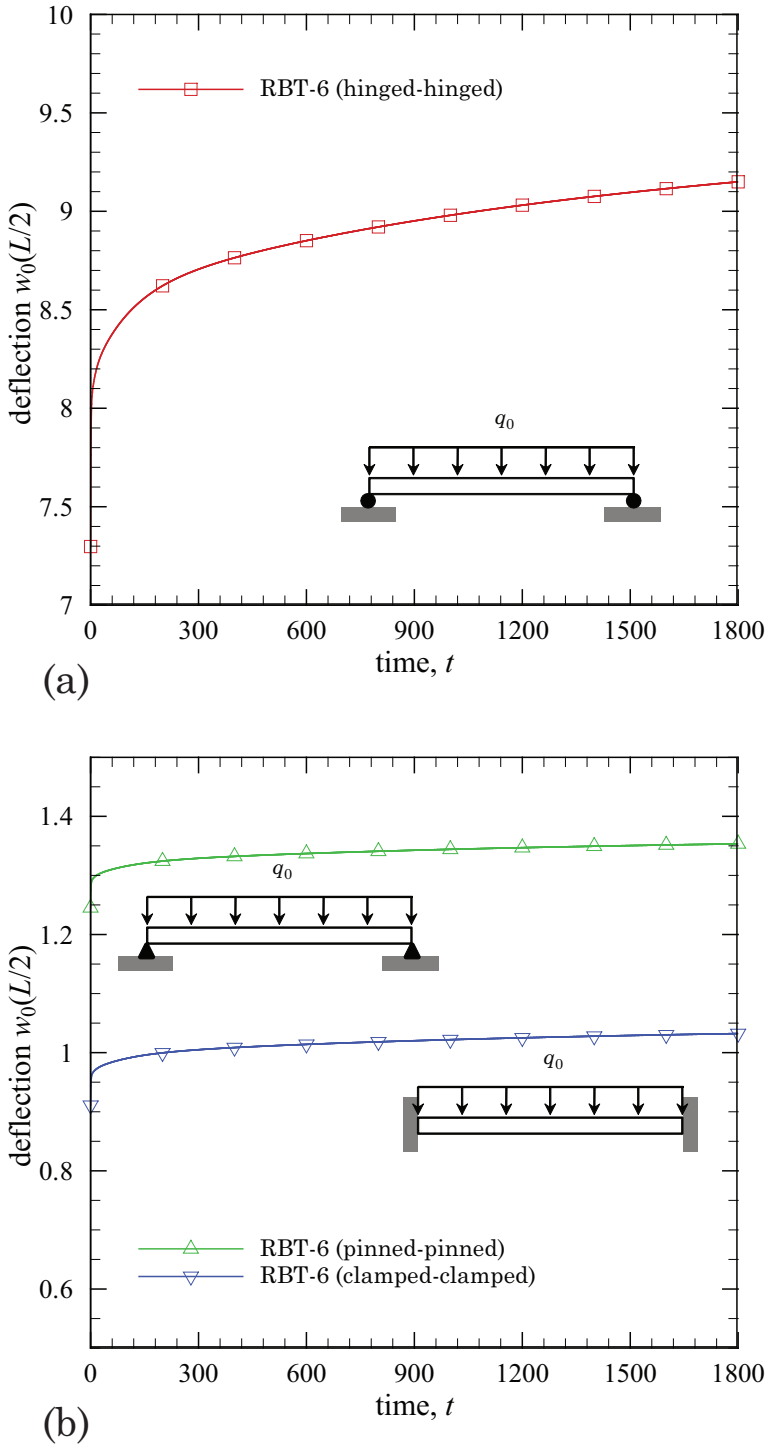

FIGURE 3. Maximum vertical deflection $w_0(L/2, t)$ of various viscoelastic beams, each subjected to a uniform vertically distributed load q_0. 2 RBT-6 elements employed in each finite element discretization: (a) hinged-hinged beam configuration and (b) pinned-pinned and clamped-clamped beam configurations.

TABLE 2. Comparison of the quasi-static finite element solutions for the maximum vertical deflection $w_0(L/2,t)$ of viscoelastic beams subjected to a uniform load q_0 for three different boundary conditions.

Time, t	RBT-2	RBT-2-R	RBT-3	RBT-4	RBT-6
Hinged-hinged					
0	5.4740	7.2840	7.2277	7.2946	7.2980
200	6.1234	8.6052	8.5170	8.6169	8.6217
400	6.1895	8.7473	8.6552	8.7592	8.7641
600	6.2295	8.8340	8.7396	8.8460	8.8510
800	6.2615	8.9035	8.8071	8.9156	8.9207
1,000	6.2886	8.9627	8.8646	8.9748	8.9799
1,200	6.3119	9.0138	8.9143	9.0259	9.0311
1,400	6.3322	9.0584	8.9575	9.0705	9.0758
1,600	6.3499	9.0975	8.9956	9.1098	9.1150
1,800	6.3656	9.1322	9.0293	9.1445	9.1498
Pinned-pinned					
0	1.2442	1.2493	1.2452	1.2452	1.2452
200	1.3233	1.3291	1.3242	1.3242	1.3242
400	1.3313	1.3371	1.3322	1.3322	1.3322
600	1.3361	1.3420	1.3370	1.3370	1.3370
800	1.3399	1.3459	1.3409	1.3409	1.3409
1,000	1.3432	1.3492	1.3441	1.3441	1.3441
1,200	1.3460	1.3520	1.3470	1.3470	1.3469
1,400	1.3484	1.3545	1.3494	1.3494	1.3494
1,600	1.3506	1.3566	1.3515	1.3515	1.3515
1,800	1.3525	1.3585	1.3534	1.3534	1.3534
Clamped-clamped					
0	0.9037	0.9098	0.9106	0.9108	0.9109
200	0.9918	0.9992	0.9993	0.9995	0.9997
400	1.0007	1.0082	1.0083	1.0084	1.0086
600	1.0060	1.0136	1.0136	1.0138	1.0140
800	1.0103	1.0180	1.0180	1.0182	1.0183
1,000	1.0139	1.0216	1.0216	1.0218	1.0220
1,200	1.0170	1.0248	1.0247	1.0249	1.0251
1,400	1.0197	1.0275	1.0275	1.0277	1.0278
1,600	1.0221	1.0299	1.0298	1.0300	1.0302
1,800	1.0242	1.0321	1.0319	1.0322	1.0323

In Table 2 and Fig. 3 we summarize numerical results for the maximum vertical deflection of the viscoelastic beam for the three different sets of boundary conditions listed above. The tabulated results were obtained using 10 RBT-2 elements (11 nodes), 10 RBT-2-R elements (11 nodes), 5 RBT-3 elements (11 nodes), 3 RBT-4 elements (10 nodes) and 2 RBT-6

elements (11 nodes). An equal time increment of $\Delta t = 1.0$ sec. was employed for all time steps. To insure convergence of the nonlinear solution procedure, the instantaneous elastic solution (at $t = 0$ sec.) was obtained through the use of five load steps. At each subsequent time step, the finite element equations were solved iteratively using the Newton procedure without employing load stepping. Typically, only 2 or 3 Newton iterations were necessary to satisfy the nonlinear convergence criterion.

It is interesting to note that the numerical results for all finite element discretizations are comparable with the exception of the case where the beam is subjected to hinged boundary conditions at both ends. For this problem, the RBT-2 finite element clearly suffers from locking. It is evident, however, that polynomial refinement of the solution naturally alleviates the locking. In fact, the RBT-3 element is almost completely locking free. Overall we find that this element is less prone to locking (when n is small) than the Timoshenko beam element employed previously by Payette and Reddy [29]. The results obtained for the RBT-6 element are spatially fully converged and compare well with the Timoshenko beam results obtained using high-order polynomial expansions [29].

For the hinged-hinged beam configuration, the vertical deflection coincides with the exact solution of the geometrically linear theory. In Table 3 we compare numerical results obtained using 2 RBT-6 beam elements with the exact solution for the Timoshenko beam theory given by Flügge [14] as

$$w_0(L/2,t) = \frac{5q_0L^4}{384D_2}\left[1 + \frac{8(1+\nu)}{5\kappa}\left(\frac{h}{L}\right)^2\right]D(t) \tag{41}$$

where $D(t)$ is the creep compliance and κ is the shear correction factor. The error in the numerical solution due to temporal integration via the trapezoidal rule tends to over-predict the deflection of the beam as is evident in Table 3 (where numerical solutions obtained using various time increment sizes are compared).

4.2. **Quasi-static deflection of a thick beam under uniform loading.** In this next example we consider a thick (i.e., $L/h < 20$) viscoelastic beam to demonstrate the ability of the Reddy beam finite element formulation to accurately account for deformations associated with shearing. We modify the thin beam problem of the previous example by letting $L = 10$ in., $q = 25.0$ lb_f/in and $\Delta t = 1.0$ sec. All other geometric and material parameters are the same as in the previous example. In Table 4 numerical results are presented for the transverse deflection of pinned-pinned and clamped-clamped beams. The same number of elements (per element type) are employed as in the previous example. In Table 4 we also

TABLE 3. Analytical and finite element solutions for the maximum quasi-static vertical deflection $w_0(L/2,t)$ of a hinged-hinged beam under uniform transverse loading q_0.

	Maximum vertical deflection, $w_0(L/2,t)$					
Time, t	Exact	$\Delta t = 0.1$	$\Delta t = 1.0$	$\Delta t = 2.0$	$\Delta t = 5.0$	$\Delta t = 10.0$
0	7.2980	7.2980	7.2980	7.2980	7.2980	7.2980
200	8.5429	8.5437	8.6217	8.8493	10.2278	14.7260
400	8.6827	8.6835	8.7641	8.9993	10.4291	15.1493
600	8.7680	8.7689	8.8510	9.0910	10.5524	15.4107
800	8.8364	8.8372	8.9207	9.1645	10.6513	15.6214
1,000	8.8945	8.8954	8.9799	9.2270	10.7356	15.8022
1,200	8.9448	8.9456	9.0311	9.2811	10.8087	15.9597
1,400	8.9886	8.9895	9.0758	9.3282	10.8726	16.0983
1,600	9.0271	9.0280	9.1150	9.3697	10.9288	16.2210
1,800	9.0612	9.0621	9.1498	9.4064	10.9787	16.3306

compare results from the Reddy beam theory with finite element results obtained using a low order reduced integration finite element model based on the Euler-Bernoulli beam theory (which does not account for deformations associated with shearing).

TABLE 4. Comparison of the quasi-static finite element solutions for the maximum vertical deflection $w_0(L/2,t)$ of thick pinned-pinned and clamped-clamped viscoelastic beams under uniform transverse loading q_0.

	Maximum vertical deflection, $w_0(L/2,t)$					
	pinned-pinned			clamped-clamped		
Time t	EBT-2-R	RBT-2-R	RBT-6	EBT-2-R	RBT-2-R	RBT-6
0	0.07184	0.07362	0.07367	0.01459	0.01645	0.01653
200	0.08437	0.08643	0.08649	0.01724	0.01943	0.01952
400	0.08571	0.08779	0.08785	0.01752	0.01975	0.01985
600	0.08652	0.08862	0.08869	0.01769	0.01995	0.02004
800	0.08717	0.08929	0.08935	0.01783	0.02010	0.02020
1,000	0.08773	0.08985	0.08992	0.01795	0.02024	0.02033
1,200	0.08821	0.09034	0.09041	0.01805	0.02035	0.02045
1,400	0.08862	0.09076	0.09083	0.01814	0.02045	0.02055
1,600	0.08899	0.09114	0.09121	0.01822	0.02054	0.02064
1,800	0.08931	0.09147	0.09154	0.01829	0.02062	0.02072

4.3. **Quasi-static deflection of a thin beam due to time-dependent loading.** For this next example we employ the geometric parameters, material properties and hinged-hinged

boundary conditions utilized in the first numerical example. We replace the stationary uniformly distributed load with the following quasi-static transverse load

$$q(t) = q_0 \left\{ H(t) - \frac{1}{\tau(\beta - \alpha)} \left[(t - \alpha\tau)H(t - \alpha\tau) - (t - \beta\tau)H(t - \beta\tau) \right] \right\} \tag{42}$$

where $q_0 = 0.25$ lb$_\text{f}$/in, $\tau = 200$ sec. and $H(t)$ is the Heaviside function. The parameters $0 \leq \alpha \leq \beta \leq 1$ are constants whose values may be appropriately adjusted. The load function above is constant for $0 < t < \alpha\tau$ and decays linearly from $t = \alpha\tau$ to $t = \beta\tau$, after which the load is maintained at zero. We utilize the above loading function to numerically demonstrate that the finite element model correctly predicts that the viscoelastic beam will eventually recover its original configuration upon removal of all externally applied mechanical loads. The numerical solution for the problem is presented in Figure 4 for various values of α and β. It is clear that in all cases, the beam tends to recover its original configuration as t tends to infinity.

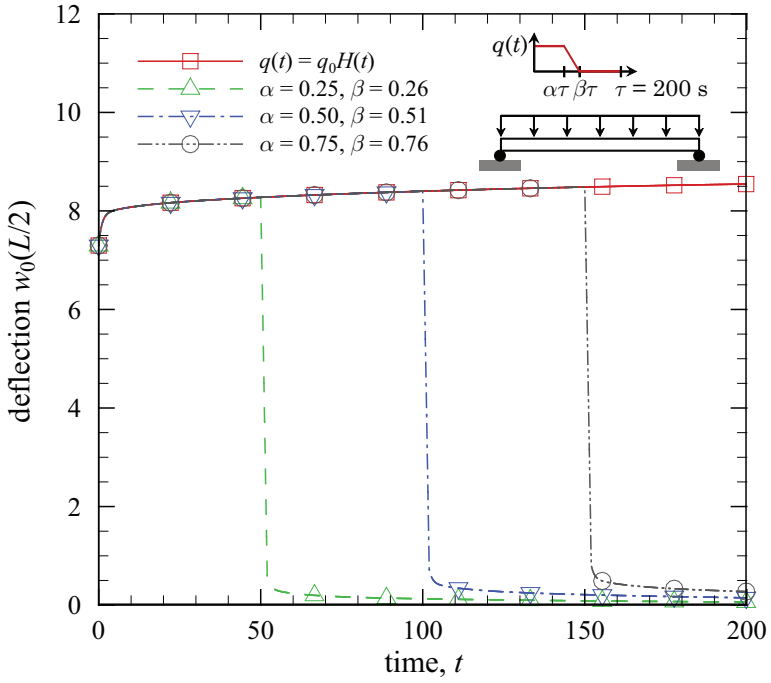

FIGURE 4. Maximum vertical deflection $w_0(L/2, t)$ of a hinged-hinged viscoelastic beam subjected to a time-dependent transverse load $q(t)$.

4.4. **Fully dynamic response of hinged viscoelastic beams.** As a final example, we consider the fully transient mechanical response of viscoelastic beams under mechanical loading. For this example we employ a simple three parameter solid model utilized previous

by Chen [8]. In the standard three parameter solid model, the relaxation modulus may be expressed as

$$E(t) = \frac{k_1 k_2}{k_1 + k_2} \left(1 - e^{-t/\tau_1^E}\right) + k_1 e^{-t/\tau_1^E} \tag{43}$$

where in the present example $k_1 = 9.8 \times 10^7$ N/m^2 and $k_2 = 2.45 \times 10^7$ N/m^2. The relaxation time is of the form $\tau_1^E = \eta/(k_1 + k_2)$ and the material density is taken to be $\rho_0 = 500$ kg/m^3. A constant Poisson ratio of $\nu = 0.3$ is assumed.

We consider a beam with hinged boundary conditions at both ends. The beam length, width and thickness are taken to be $L = 10$ m, $b = 2$ m and $h = 0.5$ m respectively. We consider two loading scenarios. In loading scenario (1) a uniformly distributed transverse load is specified along the entire length of the beam as $q(t) = q_0 H(t)$ N/m, where $q_0 = 10$. Likewise, for loading scenario (2) a periodic concentrated force is applied at the center of the beam as $F(t) = q_0 \sin(\pi t)$ N, where $q_0 = 50$. In the finite element discretization of both problems, we employ 2 RBT-6 elements of equal size. As in the previous examples, symmetry is once again exploited in construction of the finite element meshes. We utilize the Newmark-β procedure [26] for performing temporal integration of the inertia terms appearing in the fully transient beam finite element equations. The Newmark integration parameters are chosen in accordance with the constant-average acceleration method [35]. Both transient problems are solved over a total time interval of 20 sec. For loading scenario (1) we employ 500 time steps, while 1,000 time steps are utilized for loading scenario (2).

Numerical results for loading scenarios (1) and (2) are presented in Figs. 5 and 6 respectively. In each figure we present both viscoelastic and elastic solutions (where the Young's modulus is obtained by taking $E_{\text{elastic}} \equiv E(0)$). As expected, the viscoelastic effects tend to add damping to what would otherwise be purely elastic response. In Fig. 5 we present fully transient viscoelastic results using two different values for η. This problem is also solved using the quasi-static visoelasticity solution procedure. It is evident that the transient viscoelastic solution approaches the steady-state quasi-static viscoelastic response once a sufficiently long enough period of time has transpired. For loading scenario (2) the viscoelasticity effects clearly reduce the overall amplitude of the forced vibrational response. An overall smoothing of the beam response is also observed for this problem.

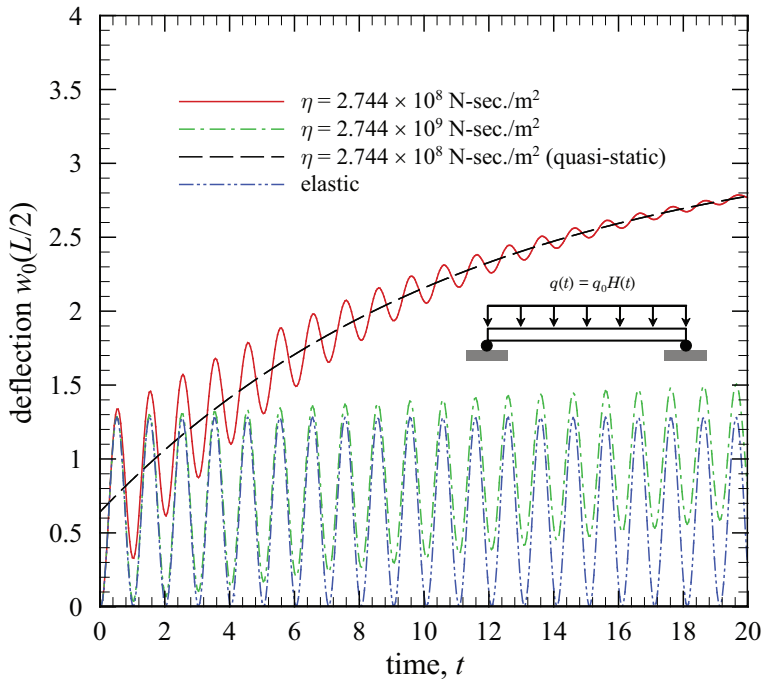

FIGURE 5. A comparison of the time-dependent vertical response $w_0(L/2, t)$ (with units of mm) of hinged-hinged beams due to a suddenly applied transverse load $q(t)$. Results are for both viscoelastic as well as elastic beams.

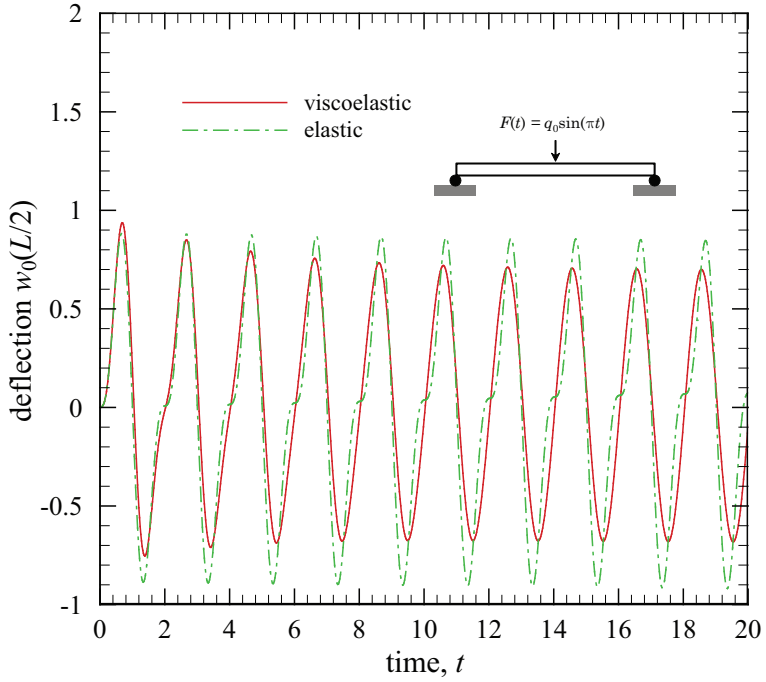

FIGURE 6. A comparison of the time-dependent vertical response $w_0(L/2, t)$ (with units of mm) of hinged-hinged viscoelastic and elastic beams due to a periodic concentrated load $F(t)$ (where $\eta = 2.744 \times 10^8$ N-sec./m^2).

5. Concluding remarks

In this paper we have presented an efficient finite element framework for the numerical simulation of the quasi-static and fully transient mechanical response of viscoelastic beam structures based on the kinematic assumptions of the third-order Reddy beam theory. The present formulation is applicable for use in the analysis of structures undergoing large transverse displacements, moderate rotations and small strains. The viscoelastic constitutive equations in the semi-discrete finite element equations were temporally discretized through the use of the trapezoidal rule and a two-point recurrence formula, resulting in an efficient temporal integration procedure. The finite element formulation has been successfully implemented numerically using standard low-order reduced integration based finite element technology as well as a family of elements constructed using high polynomial-order Lagrange and Hermite interpolation functions. The finite element procedures have been successfully employed in the numerical simulation of the mechanical response of both quasi-static and fully transient viscoelastic beams.

Acknowledgements

The research reported herein was carried out while the first author was supported by a joint graduate fellowship between Sandia National Laboratories and the Dwight Look College of Engineering at Texas A&M University. The second author acknowledges support under the MURI09 grant FA-9550-09-1-0686 from the Air Force Office of Scientific Research. The support is gratefully acknowledged. Finally, the authors would like to express their sincere gratitude to the anonymous reviewers for their constructive comments during the review process.

Appendix A: Semi-Discrete Finite Element Equation Components

The components of the partitioned element coefficient matrices and vectors appearing in the semi-discretized finite element formulation, given in Eq. (14), may be determined as

$$M_{ij}^{11} = \int_{x_a}^{x_b} I_0 \psi_i^{(1)} \psi_j^{(1)} dx \tag{A1a}$$

$$M_{ij}^{12} = M_{ji}^{21} = 0 \tag{A1b}$$

$$M_{ij}^{13} = M_{ji}^{31} = 0 \tag{A1c}$$

$$M_{ij}^{22} = \int_{x_a}^{x_b} \left(I_0 \psi_i^{(2)} \psi_j^{(2)} + c_1^2 I_6 \frac{d\psi_i^{(2)}}{dx} \frac{d\psi_j^{(2)}}{dx} \right) dx \tag{A1d}$$

$$M_{ij}^{23} = M_{ji}^{32} = -\int_{x_a}^{x_b} J_4 \frac{d\psi_i^{(2)}}{dx} \psi_j^{(1)} dx \tag{A1e}$$

$$M_{ij}^{33} = \int_{x_a}^{x_b} K_2 \psi_i^{(1)} \psi_j^{(1)} dx \tag{A1f}$$

$$K_{ij}^{11} = \int_{x_a}^{x_b} E(0) D_0 \frac{d\psi_i^{(1)}}{dx} \frac{d\psi_j^{(1)}}{dx} dx \tag{A2a}$$

$$K_{ij}^{12} = \frac{1}{2} K_{ji}^{21} = \frac{1}{2} \int_{x_a}^{x_b} \left(E(0) D_0 \frac{\partial w_0(x,t)}{\partial x} \right) \frac{d\psi_i^{(1)}}{dx} \frac{d\psi_j^{(2)}}{dx} dx \tag{A2b}$$

$$K_{ij}^{13} = K_{ji}^{31} = 0 \tag{A2c}$$

$$\begin{aligned} K_{ij}^{22} = \int_{x_a}^{x_b} \Bigg[& \frac{1}{2} E(0) D_0 \left(\frac{\partial w_0(x,t)}{\partial x} \right)^2 \frac{d\psi_i^{(2)}}{dx} \frac{d\psi_j^{(2)}}{dx} + G(0) \hat{A}_s \frac{d\psi_i^{(2)}}{dx} \frac{d\psi_j^{(2)}}{dx} \\ & + E(0) c_1^2 D_6 \frac{d^2\psi_i^{(2)}}{dx^2} \frac{d^2\psi_j^{(2)}}{dx^2} \Bigg] dx \end{aligned} \tag{A2d}$$

$$K_{ij}^{23} = K_{ji}^{32} = \int_{x_a}^{x_b} \left(G(0) \hat{A}_s \frac{d\psi_i^{(2)}}{dx} \psi_j^{(1)} - E(0) L_4 \frac{d^2\psi_i^{(2)}}{dx^2} \frac{d\psi_j^{(1)}}{dx} \right) dx \tag{A2e}$$

$$K_{ij}^{33} = \int_{x_a}^{x_b} \left(E(0) M_2 \frac{d\psi_i^{(1)}}{dx} \frac{d\psi_j^{(1)}}{dx} + G(0) \hat{A}_s \psi_i^{(1)} \psi_j^{(1)} \right) dx \tag{A2f}$$

$$\Lambda_i^1(t,s) = \int_{x_a}^{x_b} \dot{E}(t-s) D_0 \frac{d\psi_i^{(1)}}{dx} \left[\frac{\partial u_0(x,s)}{\partial x} + \frac{1}{2} \left(\frac{\partial w_0(x,s)}{\partial x} \right)^2 \right] dx \tag{A3a}$$

$$\begin{aligned} \Lambda_i^2(t,s) = \int_{x_a}^{x_b} \Bigg\{ & \dot{E}(t-s) D_0 \frac{\partial w_0(x,t)}{\partial x} \frac{d\psi_i^{(2)}}{dx} \left[\frac{\partial u_0(x,s)}{\partial x} + \frac{1}{2} \left(\frac{\partial w_0(x,s)}{\partial x} \right)^2 \right] \\ & + \dot{E}(t-s) \frac{d^2\psi_i^{(2)}}{dx^2} \left(c_1^2 D_6 \frac{\partial^2 w_0(x,s)}{\partial x^2} - L_4 \frac{\partial \phi_x(x,s)}{\partial x} \right) \\ & + \dot{G}(t-s) \hat{A}_s \frac{d\psi_i^{(2)}}{dx} \left(\frac{\partial w_0(x,s)}{\partial x} + \phi_x(x,s) \right) \Bigg\} dx \end{aligned} \tag{A3b}$$

$$\begin{aligned} \Lambda_i^3(t,s) = \int_{x_a}^{x_b} \Bigg[& \dot{E}(t-s) \frac{d\psi_i^{(1)}}{dx} \left(M_2 \frac{\partial \phi_x(x,s)}{\partial x} - L_4 \frac{\partial^2 w_0(x,s)}{\partial x^2} \right) \\ & + \dot{G}(t-s) \hat{A}_s \psi_i^{(1)} \left(\frac{\partial w_0(x,s)}{\partial x} + \phi_x(x,s) \right) \Bigg] dx \end{aligned} \tag{A3c}$$

$$F_i^1 = \int_{x_a}^{x_b} \psi_i^{(1)} f dx + \psi_i^{(1)}(x_a) Q_1 + \psi_i^{(1)}(x_b) Q_5 \tag{A4a}$$

$$F_i^2 = \int_{x_a}^{x_b} \psi_i^{(2)} q dx + Q_2 \psi_i^{(2)}(x_a) + Q_6 \psi_i^{(2)}(x_b) + Q_3 \left(-\frac{d\psi_i^{(2)}}{dx} \right) \Bigg|_{x=x_a} \tag{A4b}$$

$$+ Q_7 \left(-\frac{d\psi_i^{(2)}}{dx} \right) \Bigg|_{x=x_b}$$

$$F_i^3 = Q_4 \psi_i^{(1)}(x_a) + Q_8 \psi_i^{(1)}(x_b) \tag{A4c}$$

In the above equations we have made extensive use of the following constants

$$\begin{aligned} \hat{A}_s &= D_0 - 2D_2 c_2 + D_4 c_2^2 \\ L_4 &= c_1 (D_4 - D_6 c_1) \\ M_2 &= D_2 - 2D_4 c_1 + D_6 c_1^2 \end{aligned} \tag{A5}$$

Appendix B: History Variables and Fully-Discrete Finite Element Equation Components

The history variables in Eq. (27) may be expressed explicitly at t_{k+1} as

$$\begin{aligned} {}^1_{lm}X^1(t_{k+1}) = {} & \frac{\Delta t_{k+1}}{2} D_0 \Bigg\{ \dot{\bar{E}}_l(\Delta t_{k+1}) \left[\frac{\partial u_0(x_m, t_k)}{\partial x} + \frac{1}{2} \left(\frac{\partial w_0(x_m, t_k)}{\partial x} \right)^2 \right] \\ & + \dot{\bar{E}}_l(0) \left[\frac{\partial u_0(x_m, t_{k+1})}{\partial x} + \frac{1}{2} \left(\frac{\partial w_0(x_m, t_{k+1})}{\partial x} \right)^2 \right] \Bigg\} \\ & + e^{-\Delta t_{k+1}/\tau_l^E} {}^1_{lm}X^1(t_k) \end{aligned} \tag{B1a}$$

$${}^1_{lm}X^2(t_{k+1}) = {}^1_{lm}X^1(t_{k+1}) \tag{B1b}$$

$$\begin{aligned} {}^2_{lm}X^2(t_{k+1}) = {} & \frac{\Delta t_{k+1}}{2} \Bigg[\dot{\bar{E}}_l(\Delta t_{k+1}) \left(c_1^2 D_6 \frac{\partial^2 w_0(x_m, t_k)}{\partial x^2} - L_4 \frac{\partial \phi_x(x_m, t_k)}{\partial x} \right) \\ & + \dot{\bar{E}}_l(0) \left(c_1^2 D_6 \frac{\partial^2 w_0(x_m, t_{k+1})}{\partial x^2} - L_4 \frac{\partial \phi_x(x_m, t_{k+1})}{\partial x} \right) \Bigg] \\ & + e^{-\Delta t_{k+1}/\tau_l^E} {}^2_{lm}X^2(t_k) \end{aligned} \tag{B1c}$$

$$\begin{aligned} {}^3_{lm}X^2(t_{k+1}) = {} & \frac{\Delta t_{k+1}}{2} \hat{A}_s \Bigg[\dot{\bar{G}}_l(\Delta t_{k+1}) \left(\frac{\partial w_0(x_m, t_k)}{\partial x} + \phi_x(x_m, t_k) \right) \\ & + \dot{\bar{G}}_l(0) \left(\frac{\partial w_0(x_m, t_{k+1})}{\partial x} + \phi_x(x_m, t_{k+1}) \right) \Bigg] + e^{-\Delta t_{k+1}/\tau_l^G} {}^3_{lm}X^2(t_k) \end{aligned} \tag{B1d}$$

$$
{}^{1}_{lm}X^{3}(t_{k+1}) = \frac{\Delta t_{k+1}}{2}\left[\dot{\bar{E}}_l(\Delta t_{k+1})\left(M_2\frac{\partial\phi_x(x_m,t_k)}{\partial x} - L_4\frac{\partial^2 w_0(x_m,t_k)}{\partial x^2}\right)\right. \tag{B1e}
$$

$$
\left. +\dot{\bar{E}}_l(0)\left(M_2\frac{\partial\phi_x(x_m,t_{k+1})}{\partial x} - L_4\frac{\partial^2 w_0(x_m,t_{k+1})}{\partial x^2}\right)\right]
$$

$$
+ e^{-\Delta t_{k+1}/\tau_l^E}\,{}^{1}_{lm}X^{3}(t_k)
$$

$$
{}^{2}_{lm}X^{3}(t_{k+1}) = {}^{3}_{lm}X^{2}(t_{k+1}) \tag{B1f}
$$

Likewise, the components of the fully discretized finite element coefficient matrices and vectors, given in Eq. (28), may be evaluated at the current time step t_{k+1} as

$$
\bar{K}^{11}_{ij} = \int_{x_a}^{x_b}\left(E(0) + \frac{\Delta t_{k+1}}{2}\dot{E}(0)\right)D_0\frac{d\psi_i^{(1)}}{dx}\frac{d\psi_j^{(1)}}{dx}dx \tag{B2a}
$$

$$
\bar{K}^{12}_{ij} = \frac{1}{2}\bar{K}^{21}_{ji} = \frac{1}{2}\int_{x_a}^{x_b}\left(E(0) + \frac{\Delta t_{k+1}}{2}\dot{E}(0)\right)D_0\frac{\partial w_0(x,t_{k+1})}{\partial x}\frac{d\psi_i^{(1)}}{dx}\frac{d\psi_j^{(2)}}{dx}dx \tag{B2b}
$$

$$
\bar{K}^{13}_{ij} = \bar{K}^{31}_{ji} = 0 \tag{B2c}
$$

$$
\bar{K}^{22}_{ij} = \int_{x_a}^{x_b}\left[\frac{1}{2}\left(E(0) + \frac{\Delta t_{k+1}}{2}\dot{E}(0)\right)D_0\left(\frac{\partial w_0(x,t_{k+1})}{\partial x}\right)^2\frac{d\psi_i^{(2)}}{dx}\frac{d\psi_j^{(2)}}{dx}\right. \tag{B2d}
$$

$$
+\left(E\,(0) + \frac{\Delta t_{k+1}}{2}\dot{E}(0)\right)c_1^2 D_6\frac{d^2\psi_i^{(2)}}{dx^2}\frac{d^2\psi_j^{(2)}}{dx^2}
$$

$$
\left.+\left(G\,(0) + \frac{\Delta t_{k+1}}{2}\dot{G}(0)\right)\hat{A}_s\frac{d\psi_i^{(2)}}{dx}\frac{d\psi_j^{(2)}}{dx}\right]dx
$$

$$
\bar{K}^{23}_{ij} = \bar{K}^{32}_{ji} = \int_{x_a}^{x_b}\left[\left(G(0) + \frac{\Delta t_{k+1}}{2}\dot{G}(0)\right)\hat{A}_s\frac{d\psi_i^{(2)}}{dx}\psi_j^{(1)}\right. \tag{B2e}
$$

$$
\left.-\left(E(0) + \frac{\Delta t_{k+1}}{2}\dot{E}(0)\right)L_4\frac{d^2\psi_i^{(2)}}{dx^2}\frac{d\psi_j^{(1)}}{dx}\right]dx
$$

$$
\bar{K}^{33}_{ij} = \int_{x_a}^{x_b}\left[\left(E(0) + \frac{\Delta t_{k+1}}{2}\dot{E}(0)\right)M_2\frac{d\psi_i^{(1)}}{dx}\frac{d\psi_j^{(1)}}{dx}\right. \tag{B2f}
$$

$$
\left.+\left(G(0) + \frac{\Delta t_{k+1}}{2}\dot{G}(0)\right)\hat{A}_s\psi_i^{(1)}\psi_j^{(1)}\right]dx
$$

The quantities $\tilde{Q}_i^{\alpha}(t_{k+1})$ are expanded as

$$
\tilde{Q}_i^{\alpha} = \sum_{j=1}^{n_\alpha}{}^{j}\bar{Q}_i^{\alpha} \tag{B3}
$$

where $n_1 = 1$, $n_2 = 3$ and $n_3 = 2$, such that the components ${}^{j}\bar{Q}_i^{\alpha}$ may be defined as

$$
\begin{aligned}
{}^{1}\bar{Q}_i^{1}(t_{k+1}) = {} & \frac{\Delta t_{k+1}}{2}\int_{x_a}^{x_b} \dot{E}(\Delta t_{k+1}) D_0 \frac{d\psi_i^{(1)}}{dx}\left[\frac{\partial u_0(x,t_k)}{\partial x} + \frac{1}{2}\left(\frac{\partial w_0(x,t_k)}{\partial x}\right)^2\right] dx \\
& + \sum_{m=1}^{\text{NGP}}\sum_{l=1}^{\text{NPS}} e^{-\Delta t_{k+1}/\tau_l^E} \frac{d\psi_i^{(1)}(x_m)}{dx} {}^{1}_{lm}X^1(t_k) W_m
\end{aligned} \tag{B4a}
$$

$$
\begin{aligned}
{}^{1}\bar{Q}_i^{2}(t_{k+1}) = {} & \frac{\Delta t_{k+1}}{2}\int_{x_a}^{x_b} \dot{E}(\Delta t_{k+1}) D_0 \frac{\partial w_0(x,t_{k+1})}{\partial x}\frac{d\psi_i^{(2)}}{dx}\left[\frac{\partial u_0(x,t_k)}{\partial x}\right. \\
& \left. + \frac{1}{2}\left(\frac{\partial w_0(x,t_k)}{\partial x}\right)^2\right] dx + \sum_{m=1}^{\text{NGP}}\sum_{l=1}^{\text{NPS}} e^{-\Delta t_{k+1}/\tau_l^E} \frac{\partial w_0(x_m,t_{k+1})}{\partial x}\frac{d\psi_i^{(2)}(x_m)}{dx} \times \\
& {}^{1}_{lm}X^2(t_k) W_m
\end{aligned} \tag{B4b}
$$

$$
\begin{aligned}
{}^{2}\bar{Q}_i^{2}(t_{k+1}) = {} & \frac{\Delta t_{k+1}}{2}\int_{x_a}^{x_b} \dot{E}(\Delta t_{k+1}) \frac{d^2\psi_i^{(2)}}{dx^2}\left(c_1^2 D_6 \frac{\partial^2 w_0(x,t_k)}{\partial x^2} - L_4 \frac{\partial \phi_x(x,t_k)}{\partial x}\right) dx \\
& + \sum_{m=1}^{\text{NGP}}\sum_{l=1}^{\text{NPS}} e^{-\Delta t_{k+1}/\tau_l^E} \frac{d^2\psi_i^{(2)}(x_m)}{dx^2} {}^{2}_{lm}X^2(t_k) W_m
\end{aligned} \tag{B4c}
$$

$$
\begin{aligned}
{}^{3}\bar{Q}_i^{2}(t_{k+1}) = {} & \frac{\Delta t_{k+1}}{2}\int_{x_a}^{x_b} \dot{G}(\Delta t_{k+1}) \hat{A}_s \frac{d\psi_i^{(2)}}{dx}\left(\frac{\partial w_0(x,t_k)}{\partial x} + \phi_x(x,t_k)\right) dx \\
& + \sum_{m=1}^{\text{NGP}}\sum_{l=1}^{\text{NPS}} e^{-\Delta t_{k+1}/\tau_l^G} \frac{d\psi_i^{(2)}(x_m)}{dx} {}^{3}_{lm}X^2(t_k) W_m
\end{aligned} \tag{B4d}
$$

$$
\begin{aligned}
{}^{1}\bar{Q}_i^{3}(t_{k+1}) = {} & \frac{\Delta t_{k+1}}{2}\int_{x_a}^{x_b} \dot{E}(\Delta t_{k+1}) \frac{d\psi_i^{(1)}}{dx}\left(M_2 \frac{\partial \phi_x(x,t_k)}{\partial x} - L_4 \frac{\partial^2 w_0(x,t_k)}{\partial x^2}\right) dx \\
& + \sum_{m=1}^{\text{NGP}}\sum_{l=1}^{\text{NPS}} e^{-\Delta t_{k+1}/\tau_l^E} \frac{d\psi_i^{(1)}(x_m)}{dx} {}^{1}_{lm}X^3(t_k) W_m
\end{aligned} \tag{B4e}
$$

$$
\begin{aligned}
{}^{2}\bar{Q}_i^{3}(t_{k+1}) = {} & \frac{\Delta t_{k+1}}{2}\int_{x_a}^{x_b} \dot{G}(\Delta t_{k+1}) \hat{A}_s \psi_i^{(1)}\left(\frac{\partial w_0(x,t_k)}{\partial x} + \phi_x(x,t_k)\right) dx \\
& + \sum_{m=1}^{\text{NGP}}\sum_{l=1}^{\text{NPS}} e^{-\Delta t_{k+1}/\tau_l^G} \psi_i^{(1)}(x_m) {}^{2}_{lm}X^3(t_k) W_m
\end{aligned} \tag{B4f}
$$

Appendix C: Element Tangent Stiffness Matrix Components

The components of the element tangent stiffness coefficent matrix, given in Eq. (31), may be determined as

$$
T_{ij}^{11} = \bar{K}_{ij}^{11} \tag{C1a}
$$

$$T_{ij}^{12} = T_{ji}^{21} = 2\bar{K}_{ij}^{12} \tag{C1b}$$

$$T_{ij}^{13} = \bar{T}_{ji}^{31} = 0 \tag{C1c}$$

$$\begin{aligned} T_{ij}^{22} = \bar{K}_{ij}^{22} + \int_{x_a}^{x_b} D_0 \Bigg\{ \left(E(0) + \frac{\Delta t_{k+1}}{2} \dot{E}(0) \right) \left[\frac{\partial u_0(x, t_{k+1})}{\partial x} + \left(\frac{\partial w_0(x, t_{k+1})}{\partial x} \right)^2 \right] \\ + \frac{\Delta t_{k+1}}{2} \dot{E}(\Delta t_{k+1}) \left[\frac{\partial u_0(x, t_k)}{\partial x} + \frac{1}{2} \left(\frac{\partial w_0(x, t_k)}{\partial x} \right)^2 \right] \Bigg\} \frac{d\psi_i^{(2)}}{dx} \frac{d\psi_j^{(2)}}{dx} dx \\ + \sum_{m=1}^{\mathrm{NGP}} \sum_{l=1}^{\mathrm{NPS}} e^{-\Delta t_{k+1}/\tau_l^E} \frac{d\psi_i^{(2)}(x_m)}{dx} \frac{d\psi_j^{(2)}(x_m)}{dx} {}^{1}_{lm} X^2(t_k) W_m \end{aligned} \tag{C1d}$$

$$T_{ij}^{23} = T_{ji}^{32} = \bar{K}_{ij}^{23} \tag{C1e}$$

$$T_{ij}^{33} = \bar{K}_{ij}^{33} \tag{C1f}$$

Clearly the tangent stiffness coefficient matrix is symmetric.

References

[1] Y. Aköz and F. Kadioğlu. The mixed finite element method for the quasi-static and dynamic analysis of viscoelastic Timoshenko beams. *International Journal for Numerical Methods in Engineering*, 44(12):1909–1932, 1999.

[2] E. M. Austin and D. J. Inman. Modeling of sandwich structures. *Smart Structures and Materials 1998: Passive Damping and Isolation*, 3327(1):316–327, 1998.

[3] V. Balamurugan and S. Narayanan. Active-passive hybrid damping in beams with enhanced smart constrained layer treatment. *Engineering Structures*, 24(3):355–363, 2002.

[4] V. Balamurugan and S. Narayanan. Finite element formulation and active vibration control study on beams using smart constrained layer damping (SCLD) treatment. *Journal of Sound and Vibration*, 249(2):227–250, 2002.

[5] Y. Başar, Y. Ding, and R. Schultz. Refined shear-deformation models for composite laminates with finite rotations. *International Journal of Solids and Structures*, 30(19):2611–2638, 1993.

[6] T. Belytschko, W. K. Liu, and B. Moran. *Nonlinear Finite Elements for Continua and Structures*. John Wiley and Sons, Ltd, New York, 2000.

[7] Q. Chen and Y. W. Chan. Integral finite element method for dynamical analysis of elastic-viscoelastic composite structures. *Computers and Structures*, 74(1):51–64, 2000.

[8] T.-M. Chen. The hybrid Laplace transform/finite element method applied to the quasi–static and dynamic analysis of viscoelastic Timoshenko beams. *International Journal for Numerical Methods in Engineering*, 38(3):509–522, 1995.

[9] R. M. Christensen. *Theory of Viscoelasticity*. Academic Press, New York, 2nd edition, 1982.

[10] F. Cortés and M. J. Elejabarrieta. Finite element formulations for transient dynamic analysis in structural systems with viscoelastic treatments containing fractional derivative models. *International Journal for Numerical Methods in Engineering*, 69(10):2173–2195, 2007.

[11] M. Enelund and B. L. Josefson. Time-domain finite element analysis of viscoelastic structures with fractional derivatives constitutive relations. *American Institute of Aeronautics and Astronautics Inc*, 35(10):1630–1637, 1997.

[12] J. Escobedo-Torres and J. M. Ricles. The fractional order elastic-viscoelastic equations of motion: Formulation and solution methods. *Journal of Intelligent Material Systems and Structures*, 9(7):489–502, 1998.

[13] W. N. Findley, J. S. Lai, and K. Onaran. *Creep and relaxation of nonlinear viscoelastic materials*. North-Holland Pub. Co., New York, 1976.

[14] W. Flügge. *Viscoelasticity*. Springer, Berlin, Heidelberg, 2nd edition, 1975.

[15] A. C. Galucio, J.-F. Deü, and R. Ohayon. Finite element formulation of viscoelastic sandwich beams using fractional derivative operators. *Computational Mechanics*, 33:282–291, 2004.

[16] D. C. Hammerand and R. K. Kapania. Geometrically nonlinear shell element for hygrothermorheologically simple linear viscoelastic composites. *American Institute of Aeronautics and Astronautics Inc*, 38:2305–2319, 2000.

[17] R. Hamming. *Numerical Methods for Scientists and Engineers*. Dover Publications, Mineola, N.Y., 2nd edition, 1987.

[18] P. R. Heyliger and J. N. Reddy. A higher-order beam finite element for bending and vibration problems. *Journal of Sound and Vibration*, 126(2):309–326, 1988.

[19] A. R. Johnson, A. Tessler, and M. Dambach. Dynamics of thick viscoelastic beams. *Journal of Engineering Materials and Technology*, 119(3):273–278, 1997.

[20] G. E. Karniadakis and S. J. Sherwin. *Spectral/hp Element Methods for CFD*. Oxford University Press, Oxford, 1999.

[21] Timothy C. Kennedy. Nonlinear viscoelastic analysis of composite plates and shells. *Composite Structures*, 41(3-4):265–272, 1998.

[22] D.W. Van Krevelen. *Properties of Polymers*. Elsevier, Amsterdam, 3rd edition, 1990.

[23] J. Lai and A. Bakker. 3-D Schapery representation for non-linear viscoelasticity and finite element implementation. *Computational Mechanics*, 18:182–191, 1996. 10.1007/BF00369936.

[24] D. J. McTavish and P. C. Hughes. Finite element modeling of linear viscoelastic structures - the GHM method. In *AIAA/ASME/ASCE/AHS/ASC Structures*, Structural Dynamics and Materials Conference, pages 1753–1763, Dallas, TX; United States, April 1992.

[25] D. J. McTavish and P. C. Hughes. Modeling of linear viscoelastic space structures. *Journal of Vibration and Acoustics*, 115(1):103–110, 1993.

[26] N. M. Newmark. A method of computation for structural dynamics. *Journal of Engineering Mechanics*, 85:67–94, 1959.

[27] B. F. Oliveira and G. J. Creus. Viscoelastic failure analysis of composite plates and shells. *Composite Structures*, 49(4):369–384, 2000.

[28] A. Pálfalvi. A comparison of finite element formulations for dynamics of viscoelastic beams. *Finite Elements in Analysis and Design*, 44(14):814–818, 2008.

[29] G. S. Payette and J. N. Reddy. Nonlinear quasi-static finite element formulations for viscoelastic Euler–Bernoulli and Timoshenko beams. *International Journal for Numerical Methods in Biomedical Engineering*, 26(12):1736–1755, 2010.

[30] J. N. Reddy. A simple higher-order theory for laminated composite plates. *Journal of Applied Mechanics*, 51:745–752, 1984.

[31] J. N. Reddy. On locking-free shear deformable beam finite elements. *Computer Methods in Applied Mechanics and Engineering*, 149(1-4):113–132, 1997.

[32] J. N. Reddy. *Theory and Analysis of Elastic Plates*. Taylor and Francis, Philadelphia, 1999.

[33] J. N. Reddy. *Energy Principles and Variational Methods in Applied Mechanics*. John Wiley and Sons, Ltd, New York, 2nd edition, 2002.

[34] J. N. Reddy. *An Introduction to Nonlinear Finite Element Analysis*. Oxford University Press, Oxford, 2004.

[35] J. N. Reddy. *An Introduction to the Finite Element Method*. McGraw-Hill, New York, 3rd edition, 2006.

[36] J. N. Reddy. *An Introduction to Continuum Mechanics with Applications*. Cambridge University Press, New York, 2008.

[37] J. C. Simo and T. J. R. Hughes. *Computational Inelasticity*. Springer-Verlag, Berlin, 1998.

[38] R. L. Taylor, K. S. Pister, and G. L. Goudreau. Thermomechanical analysis of viscoelastic solids. *International Journal for Numerical Methods in Engineering*, 2(1):45–59, 1970.

[39] B. Temel, F. F. Calim, and N. Tütüncü. Quasi-static and dynamic response of viscoelastic helical rods. *Journal of Sound and Vibration*, 271(3–5):921–935, 2004.

[40] M. A. Trindade, A. Benjeddou, and R. Ohayon. Finite element modelling of hybrid active-passive vibration damping of multilayer piezoelectric sandwich beams-part I: Formulation. *International Journal for Numerical Methods in Engineering*, 51(7):835–854, 2001.

[41] C. M. Wang, J. N. Reddy, and K. H. Lee. *Shear Deformable Beams and Plates. Relationships with Classical Solutions*. Elsevier, Amesterdam, 2000.

[42] Z. Zheng-you, L. Gen-guo, and C. Chang-jun. Quasi-static and dynamical analysis for viscoelastic Timoshenko beam with fractional derivative constitutive relation. *Applied Mathematics and Mechanics*, 23:1–12, 2002.

Correspondence to: Mr. Gregory S. Payette, Graduate student, Department of Mechanical Engineering, Texas A&M University, College Station, Texas - 77843. TEL:+1-979-862-2417

E-mail address: paye4446@tamu.edu

Dr. J. N. Reddy, Department of Mechanical Engineering, Texas A&M University, 210 Engineering/Physics Building, College Station, Texas - 77843. TEL:+1-979-862-2417

E-mail address: jnredddy@tamu.edu